Quantitative microdiffraction from deformed crystals with unpaired dislocations and dislocation walls

R. I. Barabash, G. E. Ice, and F. J. Walker

Citation: Journal of Applied Physics **93**, 1457 (2003); doi: 10.1063/1.1534378
View online: http://dx.doi.org/10.1063/1.1534378
View Table of Contents: http://scitation.aip.org/content/aip/journal/jap/93/3?ver=pdfcov
Published by the AIP Publishing

Quantitative microdiffraction from deformed crystals with unpaired dislocations and dislocation walls

R. I. Barabash,[a] G. E. Ice, and F. J. Walker
Metals and Ceramics Division, Oak Ridge National Laboratory, Oak Ridge, Tennessee 37831-6118

(Received 10 June 2002; accepted 8 November 2002)

This article describes how unpaired dislocations alter white-beam Laue patterns for either isolated dislocations, dislocation walls, or combinations of dislocation walls and isolated dislocations. The intensity distribution of Laue diffraction is analyzed as a function of local misorientation. We show how to quantitatively determine the dislocation structure of single crystals and polycrystals with plastic deformation. The technique is applied to interpret the complicated plastic–elastic field in an iridium weld sample. [DOI: 10.1063/1.1534378]

I. INTRODUCTION

Polychromatic x-ray microdiffraction offers an approach to the study of mesoscale dynamics in polycrystalline materials.[1–3] As a polychromatic x-ray beam penetrates a sample, it produces a Laue pattern from each subgrain that it intercepts [Fig. 1(a)]. The intensity at each position in the Laue pattern is proportional to a line integral through reciprocal space weighted by the incident spectrum. The Laue pattern is sensitive to grain orientation, unit cell shape, and deformation. Polychromatic microdiffraction has major advantages over traditional monochromatic diffraction for micron scale spatial resolution because no sample rotations are required; furthermore, the depth at which the scattering originates can be resolved through a differential aperture microscopy technique.[2] In addition to providing precise information on the phase, grain orientation, and morphology of polycrystalline materials, polychromatic microdiffraction is sensitive to elastic and plastic distortion. As illustrated in previous papers, the deviatoric strain tensor can be recovered with x-ray Laue methods, and the full elastic strain tensor can be recovered if the energy (wavelength) of one reflection is measured.[2–4]

It has also been shown previously that quantitative information on the number and kind of unpaired random dislocations can be recovered from streaking in Laue images.[5] A general kinematic treatment of polychromatic x-ray scattering by crystals with random unpaired dislocations has been presented in Ref. 5. This approach is appropriate for analysis of deformation where a kinematic description of scattering is a valid approximation. Here, we summarize the key features of the earlier paper and extend the approach to cases where the dislocations are organized into dislocation walls. With this formalism, the diffraction from plastically deformed materials with random unpaired dislocations, dislocation walls, or combinations of unpaired dislocations and dislocation walls, can all be modeled.

As an example, we apply our deformation analysis to an Ir weld sample. Welded grains show an interesting deformation pattern that depends on the thermal history of a grain and on the local boundary conditions. Previous studies of deformation in these materials were based on electron backscatter diffraction methods;[6] however, until recently, nondestructive three-dimensional analysis of plastic deformation with micron resolution was not possible for bulk materials. Here, we illustrate how the 12 most likely dislocation systems in a face-centered-cubic sample can produce distinctive streaking in a polychromatic microdiffraction image and how the measured streaking can be used to quantitatively determine the local deformation tensor with subgrain resolution in an Ir weld.

II. INDEXING AND PSEUDOSTEREOGRAPHIC PROJECTION OF LAUE PATTERN

In traditional white-beam Laue diffraction, a continuum spectrum is diffracted by a single crystal (or single grain). The crystal scatters the beam into a characteristic Laue pattern that depends on the crystal space lattice, its orientation, and the incident-beam energy distribution [Fig. 1(b)]. Each characteristic reflection hkl is scattered specularly from the crystal planes hkl, which allows the planar orientations with respect to the incident beam to be determined directly. The incident spectral distribution can be described by $I_0(k)$ where $(k=|\mathbf{k}_0|)$. In reciprocal space the exact positions of regular reflections (hkl) are related to the orientation, space lattice, and to the real-space unit cell size. The momentum transfer corresponding to a Bragg/Laue reflection $\mathbf{G}_{hkl}$ we define as $\mathbf{G}_{hkl}=\mathbf{k}_{hkl}-\mathbf{k}_0$, where $(|\mathbf{k}_0|=|\mathbf{k}_{hkl}|=k)$. Here, $\mathbf{k}_0$ is the incident wave vector and $\mathbf{k}_{hkl}$ is the scattered wave vector that satisfies the Bragg/Laue conditions. The diffusely scattered intensity about the centroid of the Laue spot depends on the deviation $\mathbf{q}=\mathbf{Q}-\mathbf{G}_{hkl}=\mathbf{k}-\mathbf{k}_{hkl}$ between the diffraction vector $\mathbf{Q}=\mathbf{k}-\mathbf{k}_0$, and the momentum transfer $\mathbf{G}_{hkl}$ for a Laue reflection. For each wavelength of radiation λ, the center of the Ewald sphere (C) and the origin in reciprocal space (O), are separated by the distance $1/\lambda$. This distance is different for each reflection hkl and corresponds to different Ewald spheres; this complicates the analysis for polychromatic beams. We write the Laue equation in a manner that takes into account the λ spectrum in the beam.

[a]Electronic mail: barabashr@ornl.gov

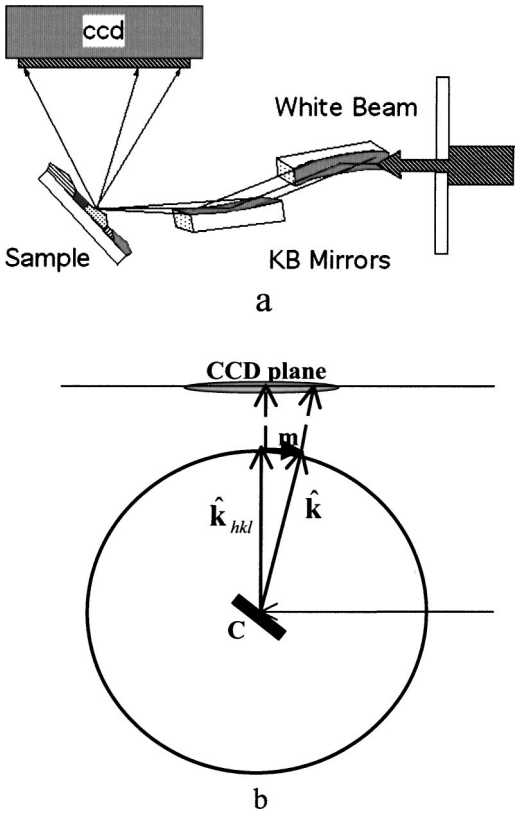

FIG. 1. Experimental setup for white-beam Laue diffraction (a) and formation of Laue images as a function of the misorientation vector **m** between radial integrals around a Bragg peak (b).

The scattering angle into each pixel is calibrated to a few parts in 10^5. The Laue pattern is then indexed[4] to determine the unit cell orientation with respect to a model basis. A rotation matrix is then used to go from the sample to the unit cell basis. In nondistorted crystals each Laue reflection with incident beam $\mathbf{k}_0$ and diffracted beam $\mathbf{k}_{hkl}$ determines the direction of the Bragg plane normal $\mathbf{G}_{hkl}$.[4,7–10] The Bragg plane normal and 2ϑ Bragg angle for each reflection are fixed and compared to possible pairs of indices for the sample crystal structure. To simplify the computation, we project the reciprocal lattice space directions onto the m_x, m_y plane. This projection, as opposed to a more standard stereographic projection, is used for the analysis of experimental results in Figs. 5 and 6.

III. MODEL OF DISLOCATION ARRANGEMENTS

We follow the concept of the cell-block structure first introduced by Mughrabi and co-workers[11] and further developed in a number of papers (see, for example, Ref. 12). We restrict ourselves to models where the unpaired edge dislocations have one of three organizations: (1) random geometrically necessary (unpaired) dislocations (GNDs); (2) unpaired geometrically necessary boundaries (GNBs) formed by thin dislocations walls; and (3) GNBs separating regions with incidental dislocation boundaries (IDB) and individual GNDs. A sketch of these structures is presented at Fig. 2.

Consider the set of edge dislocations illustrated in Fig. 2. Dislocations from this set have Burgers vectors $\mathbf{b_i}$ parallel to

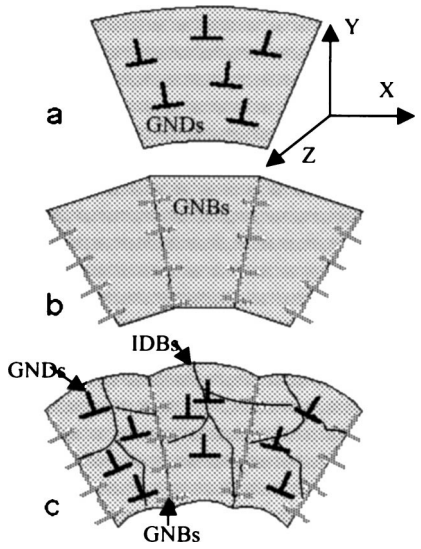

FIG. 2. Schematic of crystals with local rotations caused by different arrangements of unpaired dislocations: (a) randomly distributed individual unpaired dislocations (GNDs); (b) randomly distributed tilt dislocation walls (GNBs); and (c) randomly distributed tilt dislocation boundaries (GNBs) with randomly distributed individual unpaired dislocations (GNDs) and incidental dislocation boundaries (IDBs) in inner regions.

the X axis and dislocations lines τ parallel to the Z axis. For an equal number of random "$+\mathbf{b}$" and "$-\mathbf{b}$" dislocations, the average deformation tensor is negligible. Broadening of the diffuse scattering is induced by random local fluctuations in the unit cell orientations and d spacing that tend to cancel out over long length scales.

To describe the distribution of dislocations, we introduce the number c_t. It can take two values:

$$c_t=\begin{cases}1, & (+)\\ 0, & (-)\end{cases}.$$

If there is a dislocation in the position t, the corresponding number $c_t=1$, and in positions without dislocations $c_t=0$. Each edge dislocation creates a displacement field with displacement $\mathbf{u}_{it}$ of the ith scattering cell in the plane XOY perpendicular to its line. The projections of the displacement vector in this plane for the simple case of elastically isotropic crystals, are described by the following equations:[13]

$$u_x=\frac{b}{2\pi}\left[\tan^{-1}\frac{y}{x}+\frac{xy}{2(1-\mu)(x^2+y^2)}\right], \tag{1a}$$

$$u_y=-\frac{b}{2\pi}\left[\frac{1-2\mu}{2(1-\mu)}\ln(x^2+y^2)+\frac{(x^2-y^2)}{4(1-\mu)(x^2+y^2)}\right]. \tag{1b}$$

Here, μ is Poisson's ratio. The total displacement of ith cell $\mathbf{u}_i$ is due to superposition of all dislocations and is defined by the equation[14]

$$\mathbf{u}_i=\sum_t c_t\mathbf{u}_{it}. \tag{2}$$

For unpaired dislocations (Fig. 2), the mean deformation tensor can be written in terms of the antisymmetric Levi–Civita tensor of third rank $\epsilon_{\tau lm}$ and a dislocation density tensor of second rank ρ_m:[5,14]

$$\epsilon_{\tau lm}\left(\frac{\partial \omega_{mn}}{\partial x_l}\right)=-\rho_{\tau n}. \tag{3}$$

Here, the Levi–Civita tensor has elements $\epsilon_{123}=\epsilon_{231}=\epsilon_{312}=1$; $\epsilon_{213}=\epsilon_{132}=\epsilon_{321}=-1$; and all other $\epsilon_{ijk}=0$. The tensor of dislocation density $\rho_{\tau n}$ has indices τ that specify the crystallographic direction of the dislocation line, and indices n that specify the Burgers vector direction. For a general set of dislocations with dislocation density n^+, unit line directions τ, and Burgers vector components b_x, b_y, b_z, we write the tensor of dislocation density as

$$\rho_{ij}=n^+\begin{pmatrix}\tau_x b_x & \tau_x b_y & \tau_x b_z\\ \tau_y b_x & \tau_y b_y & \tau_y b_z\\ \tau_z b_x & \tau_z b_y & \tau_z b_z\end{pmatrix}. \tag{4}$$

For example, with edge dislocations, as shown in Fig. 2(a), $\tau=(001)$, $n=(100)$, and there is only one nonzero component, $\rho_{zx}=n^+b$. From Eqs. (3) and (4) it follows that there are only two nonzero components of the mean deformation tensor: $\omega_{xy}=-\omega_{yx}=n^+bx$. We note that this distortion field is antisymmetric and represents a pure rotation about the Z axis that increases with displacement in x. Other systems of edge, screw, or mixed dislocations can be similarly treated, but for the following discussion we restrict ourselves to edge dislocations.

In real crystals individual GNDs tend to group into walls to reduce the stored energy.[11–19] Consider the structure with geometrically necessary randomly distributed tilt dislocation boundaries (GNBs) [Fig. 2(b)]. Each wall provides a rotation between two neighboring mosaic blocks around the line of the wall. Unit vector $\boldsymbol{\omega}$ parallel to the rotation axis of each wall coincides with unit vector $\boldsymbol{\tau}$ along the dislocation lines in the case of a tilt boundary. We consider pure tilt boundaries formed by equidistant edge GNDs (so-called ''thin walls''). These boundaries do not produce long-range elastic strain but generate subgrain rotations. The remaining stresses in the GNB region are periodic with a wavelength $b^*=b\csc\Theta/2$. These stresses are only appreciable at distances shorter than within b^* from the GNB.[13] If h is the distance between these dislocations in the wall, one can consider the boundary as a single defect producing the local rotation field Θ. The misorientation angle Θ due to the boundary is defined by the equation $b/h=2\sin\Theta/2$, where $b/h\approx\Theta$ for small angle GNBs. To characterize this model quantitatively we define the average distance D between GNBs and write the number of GNBs per unit length as $1/D$. The total density of GNDs grouped in the GNBs is denoted by $n^+=1/Dh$. We define an axis X perpendicular to the plane of the wall, and an axis Z parallel to the direction of dislocation lines in the wall. For this coordinate system (Fig. 2), two nonzero components of the mean deformation tensor are equal: $\omega_{xy}=-\omega_{yx}=\Theta x/D$. This mean deformation tensor again results in pure rotations about the Z axes. The rotations increase with displacement in x. The number of GNBs per unit length and the length of the crystal in the X direction determine the total rotation of the lattice.

Generally, real crystal contains a hierarchy of dislocation structures. Some of the GNDs are distributed randomly, and the rest may form different kinds of nonrandom arrangements IDBs and GNBs. It has been found that dislocation boundaries evolve within a regular pattern of grain subdivision on two scales.[16,17] The smaller scale is related to the usual cell boundaries—so-called incidental dislocation boundaries. The larger scale is related to long and continuous so-called geometrically necessary dislocation boundaries. Usually, GNBs separate volume elements, which deform by different slip system modes with different strain amplitudes.[16,17] Typically there are many IDBs separating ordinary dislocation cells between two cell-block boundaries formed by GNBs [Fig. 2(c)].

IV. LAUE DIFFRACTION BY CRYSTALS WITH GEOMETRICALLY NECESSARY DISLOCATIONS

A. Intensity distribution of Laue diffraction as a misorientation distribution function

Dislocations change the diffraction conditions and enlarge the region of high intensity around each Bragg position. The intensity distribution of a crystal with dislocations may be written as follows:[5,14,15]

$$I(\mathbf{q})=f^2\sum_{i,j}\ e^{i\mathbf{q}\cdot R_{ij}}e^{-T},\quad T=nS\sum_t\ 1-e^{[i\mathbf{Q}\cdot(\mathbf{u}_{it}-\mathbf{u}_{jt})]}. \tag{5}$$

Here, f is the average scattering factor; $\mathbf{R}_{ij}=\mathbf{R}_i^0-\mathbf{R}_j^0$ is the distance vector between the lattice cells i, j in the undistorted virtual crystal; S is the area of one dislocation in a transverse plane; n is the total dislocation density; and nS is a dimensionless quantity that indicates the fraction of lattice sites covered with dislocations. Correlation function T differs for different dislocation arrangements. In the most general case it contains both real and imaginary parts. The intensity distribution $I(q)$ of x-ray (or neutron) scattering due to defects can be computed from the expression

$$I(\mathbf{Q})=\left|\sum_i\ f_i\exp[i\mathbf{Q}\cdot(\mathbf{R}_i^0+\mathbf{u}_i)]\right|^2. \tag{6}$$

Here, f_i is the scattering factor from an individual atom i, with relaxed coordinates $R_i=\mathbf{R}_i^0+\mathbf{u}_i$ due to the presence of defects. Here, $\mathbf{u}_i$ is the displacement from the equilibrium positions $\mathbf{R}_i^0$ corresponding to the undeformed crystal. We calculate $\mathbf{u}_i$ using continuum elastic theory. In Laue diffraction, the incident beam and scattered beam directions define a line in reciprocal space. The position along this line is determined by the wavelength of the scattered radiation. For example, reciprocal lattice points $(00h)$, $(002h)$, $(003h)$, etc., are scattered towards the same pixel on a charge-coupled device but lie at different positions radially in reciprocal space. To analyze the white-beam intensity distribution from a deformed grain, we introduce *unit* vectors in each direction of scattering $\hat{\mathbf{k}}=\mathbf{k}/|\mathbf{k}|$. We define a special misorientation vector $\mathbf{m}$ near a Bragg reflection $\mathbf{m}=\hat{\mathbf{k}}-\hat{\mathbf{k}}_{hkl}$. Mis-

orientation vector **m** gives the difference between the unit vector parallel to Bragg reflection (hkl) and an arbitrary direction in its vicinity [Fig. 1(b)]. Note that this is a crucial difference between the general intensity distribution in the reciprocal space and intensity distribution of a scattered Laue beam.

The region of high intensity around each vector $\hat{\mathbf{k}}_{hkl}$ in Laue geometry $I_L(\mathbf{m})$ is a function of a misorientation vector. Within this approximation, the resulting intensity distribution by the deformed crystal in the white microbeam method can be written as follows:

$$I_L(\mathbf{m}) \cong A \int I_0(k) I(\mathbf{q}) dk,$$
$$\mathbf{q} = |\mathbf{k}_{hkl}| \mathbf{m}_{\perp} + (|\mathbf{k}_{hkl}| \mathbf{m}_{\mathrm{rad}} + \Delta k \mathbf{G}/|\mathbf{k}_{hkl}|). \tag{7}$$

Here, $|\mathbf{k}_{hkl}|$ is the radius of the Ewald sphere that passes through $\mathbf{G}_{hkl}$, A is a constant, and $\mathbf{m}_{\mathrm{rad}}$ and $\mathbf{m}_{\perp}$ are components of misorientation vector **m** along and perpendicular to the direction of the scattered beam $\hat{\mathbf{k}}_{hkl}$. Misorientation vector **m** characterizes Laue intensity $\mathbf{I}_L(\mathbf{m})$ assuming the wavelength varies smoothly near the Bragg energy. Information about the radial diffuse scattering distribution is lost unless the Laue pattern is differentiated in wavelength (energy scanning incident beam). The second equation in Eq. (7) is valid when $\Delta k/|k_0| \ll 1$. In the first approximation, orientation vector **m** is perpendicular to $\hat{\mathbf{k}}_{hkl}$ [Fig. 1(b)].

In our experimental setup the microfocusing optics introduce a small $\leqslant 1$ mrad convergence to the incident beam. This convergence angle has a negligible effect along a streak, but can change the intensity distribution in the narrow direction of the streak. $\mathbf{I}_L(\mathbf{m})$ should, therefore, be convoluted with the experimental angular resolution function.

B. Correlation function and full width at half maximum for Laue intensity distribution

Following the approach described in the Refs. 18 and 19, the difference between displacements of two scattering lattice cells i and j can be written as

$$\mathbf{u}_{it} - \mathbf{u}_{jt} = (\mathbf{R}_{ij}\nabla)\mathbf{u}_{it} + \tfrac{1}{2}(\mathbf{R}_{ij}\nabla)^2 \mathbf{u}_{it}, \quad \text{where} \quad \nabla \equiv \nabla_{R_i}. \tag{8}$$

Correlation function T [Eq. (5)] can be expanded with respect to small displacements. In general, an arbitrary distribution of paired and unpaired dislocations has both real and imaginary parts $T = T_1 + T_2 + T_3$:

$$T_1 = i \sum_{ti} c_i (\mathbf{R}_{ij}\nabla)(\mathbf{G}_{hkl}\mathbf{u}_{it}),$$
$$T_2 = -\sum c_i \{1 - \cos[(\mathbf{R}_{ij}\nabla)(\mathbf{G}_{hkl}\mathbf{u}_{it})]\}, \tag{9a}$$
$$T_3 = \frac{i}{2} \sum_{it} c_i \cos[(\mathbf{R}_{ij}\nabla)(\mathbf{G}_{hkl}\mathbf{u}_{it})](\mathbf{R}_{ij}\nabla)^2 (\mathbf{G}_{hkl}\mathbf{u}_{it}). \tag{9b}$$

The first term T_1 is imaginary, linear with respect to the density of unpaired dislocations n^+ and goes to zero when $n^+ = 0$. The real part of correlation function T_2 is independent of whether dislocations are paired or unpaired. Part T_3 is imaginary and with $T_3 \ll T_1$ it may be neglected. With substitution of Eqs. (1a), (1b), (2) and (8) into (9a) and (9b), we find that for unpaired dislocation densities in system λ of n_λ^+,

$$T_1 = -iC_1 \sum_{\lambda} n_\lambda^+ (\mathbf{R}_i \cdot \mathbf{b}_\lambda)([\mathbf{Q}^* \mathbf{R}_{ij}]\boldsymbol{\tau}_\lambda),$$
$$T_2 = C_2 (Qb)^2 \ln L \sum_{\lambda} n_\lambda \varphi_\lambda. \tag{10}$$

Here, C_1, C_2 are the contrast factors, λ is the number of the dislocation slip system, L is the size of the subgrain (or the cutoff radius), and φ_λ is the orientation factor for each dislocation system. From the structure of Eq. (10) it follows that dislocations parallel to the diffraction vector do not contribute to function T_1 and do not influence the intensity of scattering (contrast factor C_1 for these dislocations is zero). T_2 describes the influence of mean distortions due to randomly distributed individual GNDs.

For an equal number of random "$+\mathbf{b}$" and "$-\mathbf{b}$" dislocations the broadening of the diffuse scattering is induced by random local fluctuations in the unit cell orientations and d spacing that tend to cancel out over long length scales. Due to the character of the displacement field around edge GNDs, displacements occur only in planes perpendicular to the direction of dislocation lines τ. As a result, coherence is not changed along direction τ, and the diffuse intensity in this direction is the same as for crystals without dislocations. Perpendicular to τ, the diffuse distribution is roughly symmetric with a characteristic full width at half maximum (FWHM) dependent on the total dislocation density n: FWHM$\propto \sqrt{n}$. For GNDs [Fig. 2(a)], the diffuse scattering distribution relates distortion tensor ω_{ij}, due to GNDs, n^+, to the dislocation density and system (direction τ, and Burgers vector **b**).

C. Natural axes of the Laue spot

Near a Laue spot, we define two natural axes ξ and ν: $\xi = \tau \times \mathbf{g}/|\tau \times \mathbf{g}|$, and $\nu = \xi \times \mathbf{g}/|\xi \times \mathbf{g}|$ perpendicular to the unit vector in the direction of momentum transfer **g**. We have previously modeled lattice rotations and diffuse scattering for a single Laue spot[5] associated with geometrically necessary (unpaired) individual dislocations. Such a structure is shown at Fig. 2(a). As in Ref. 5 with this coordinate system, the diffuse scattering is strongly elongated in the ξ direction. The full width at half maximum in the ξ direction FWHM$_\xi$ depends on the average distance between GNBs, their mutual orientation with momentum transfer $\mathbf{G}_{hkl}$, the type of GNB (tilt or twist), and the incident x-ray beam direction. In the second transverse direction ν, FWHM$_\nu$ depends on the total number of boundaries per unit length b/D and usually FWHM$_\nu \ll$ FWHM$_\xi$. Significantly, if multiple systems are simultaneously active, the width of the Laue spot perpendicular to the major axis of streaking can be large. We emphasize that in white-beam diffraction the FWHM is a function of misorientation vector **m** between unit vectors (rather than the reciprocal space momentum transfer vector).

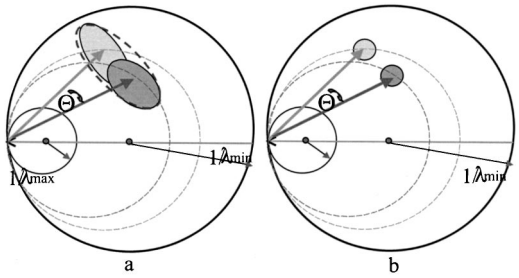

FIG. 3. Splitting of Laue reflections into sharp peaks for two extreme values of Eq. (11): (a) continuous distribution ($K<1$); and (b) spot splits into separate peaks ($K>1$).

D. Splitting of the Laue intensity distribution

If the angular misorientation between GNBs is sufficiently large, the reflection becomes discontinuous. To understand this dependence, we assume that along penetration depth L the x-ray beam intersects several fragments with average size D_{fr}. Each fragment contributes to the diffraction. The number of such contributions is L/D. Each boundary produces an average misorientation Θ. The average distance between the Laue maximums, formed by two adjacent fragments is $\Delta=(Q/k_0)\Theta$. If this distance exceeds the average $\mathrm{FWHM}_{\mathrm{fr}}$ of the Laue image for each fragment along the ξ axis, the Laue spots split (Fig. 3). If almost all dislocation walls are unpaired, the following criterion can be used:

$$K=\left(\frac{\Theta Q}{k_0\ \mathrm{FWHM}_{\mathrm{fr}}}\right). \tag{11}$$

If $K<1$, the intensity distribution of the white-beam reflection is continuous. If $K>1$, the white-beam reflection is split into separate spots. The intensity profile along the streak consists of several spikes.

E. Comparison of Laue patterns from grains with random dislocations to Laue patterns from grains with boundary dislocations

Unpaired boundary and individual dislocations can have either similar or distinctive effects on the Laue pattern. Both organizations of dislocations result in streaking of Laue reflections. The same orientation of GNDs and GNBs corresponds to the same direction of streaking. However, GNDs cause continuous and GNBs discontinuous intensity distributions along the streak. Due to local strains, individual dislocations influence the length of the streak more than the same number of dislocations in a boundary. Moreover, the FWHM in the narrow direction of the streak is most strongly influenced by individual dislocations and can be used to separate boundary dislocations from the ones inside the fragment. For better separation of unpaired boundary and individual dislocations, the white x-ray microbeam intensity should be differentiated with respect to $|\mathbf{k}_0|$. It can be done by scanning the incident x-ray energy with an incident beam monochromator.

To understand the main features of white-beam scattering from crystals with various dislocation arrangements, we simulated the intensity of scattering by crystals with different numbers of fragments (Fig. 4). To simplify the interpretation of the patterns, the total number of excess dislocations was kept constant. A total dislocation density of $n^+=10^{12}\,\mathrm{cm}^{-2}$ was chosen. This value is typical of highly deformed crystals. In the first simulation, all dislocations are randomly distributed. The deformation fields around each dislocation are superimposed and the intensity was calculated from Eq. (7). The corresponding intensity profile broadens predominantly along the ξ axis with a typical ''flattop'' shape [Fig. 4(a)]. As dislocations are removed from the fragments and added to the dislocation walls, a *correlated* misorientation develops between the neighboring parts of the crystal. When the dislocation walls are well developed, so that the distance between dislocations within wall h is much shorter than the distance between the walls $D(h\ll D)$ (corresponding to the case when 75% of all dislocations are grouped within the walls), the intensity distribution becomes discontinuous [Fig. 4(c)]. Such walls produce sharp rotations of the crystal fragments with an abrupt rotational phase variation. In real crystals with dislocation walls there is a transition layer providing a smooth rotation from one fragment to another.[14] For sharp ''thin'' walls the volume fraction of the transition layer is small. For constant n^+ the number of sharp ''thin' dislocation walls does not alter the total misorientation. However, when the walls are not well developed, as in the case of 25%–5% of the total number of dislocations grouping within the walls [Figs. 4(a) and 4(b)], the opposite condition is true, $h\cong D$. Here, each fragment still contains many randomly distributed dislocations and has a large FWHM_{ξ}. This results in overlapping of the spikes and the total FWHM_{ξ} are large. For a relatively large number of walls, the scattering from each fragment blends together. For higher resolution measurements, a larger number of separate spots can be detected within a streak, as observed experimentally. This simulation illustrates that observed splitting of a white-beam reflection (hkl) into spots depends on the following parameters: density of excess dislocations inside the wall, misorientation angle created by dislocation subboundary, number of walls in the irradiated volume, size of a fragment, size of scattering volume, and the experimental resolution function. With higher resolution the experimental intensity distribution reveals more spikes. The results of simulated scattering by general dislocation structures (when some fraction of dislocations is grouped into the walls and some of them are randomly distributed in the inner regions) are illustrated in the next section.

Based on the analysis above we can make the following generalizations:

• If $n^+L\gg 0.1\sqrt{nl}$, the intensity of scattering with white microbeam diffraction is mainly influenced by the unpaired GND and GNB (related to correlated deformations of the lattice). For example, this condition is valid if $L=1\ \mu\mathrm{m}$, $n=10^{11}\,\mathrm{cm}^{-2}$, and $n^+=n$. In this case, $\mathrm{FWHM}_{\xi}\gg\mathrm{FWHM}_{\nu}$ and the inherent energy weighted integral is representative of the key features of $I(\mathbf{q})$. It is also possible to analyze the main features of the unpaired dislocation structure of the material.

• In the opposite case, $\mathrm{FWHM}_{\xi}\sim\mathrm{FWHM}_{\nu}$ and the inten-

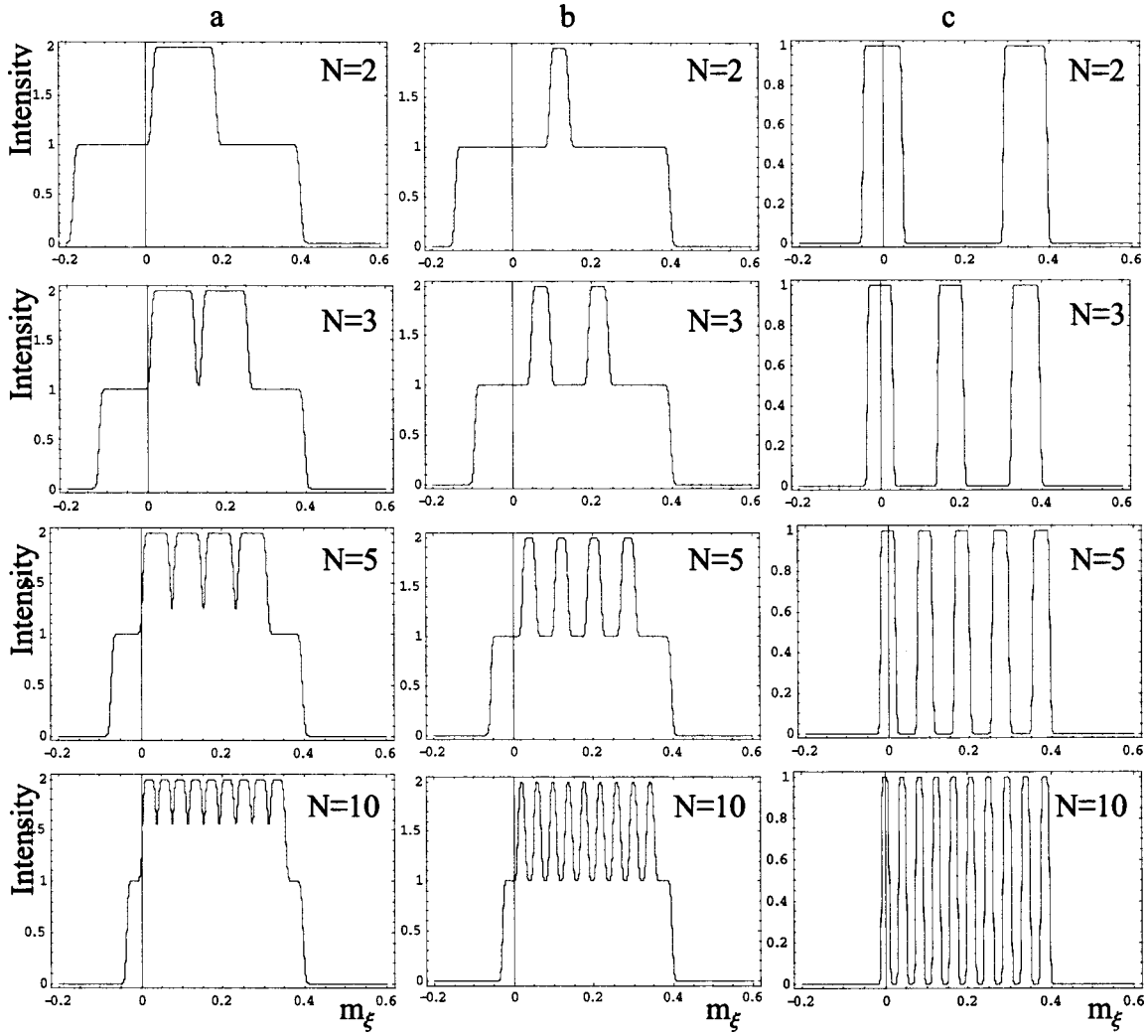

FIG. 4. Simulated intensity profiles along the Laue streaks with various groupings of the dislocations into walls separating the fragments: (a) 5% of all dislocations group into the walls; (b) 25% of all dislocations group into the walls; and (c) 75% of all dislocations group into the walls. The numbers of fragments are indicated on the left side of the figure.

sity distribution is almost isotropic. Here, the intensity of scattering measured in a white microbeam experiment is significantly influenced by the total dislocation density in both directions. In this case, a detailed knowledge of intensity distribution in three-dimentioned (3D) reciprocal space is necessary to adequately understand the dislocation structure. For this case the white x-ray microbeam intensity should be differentiated with respect to $|\mathbf{k}_0|$.

• When the observable intensity variations are measurable along the streak ($K>1$), the dislocation structure must be predominantly restricted by unpaired dislocation walls forming GNBs with some number n^+ of unpaired GND between them.

• For the same number of dislocations the FWHM_ξ can differ by up to ~50% depending on the hierarchical arrangement of n^+.

V. PLASTIC DEFORMATION NEAR AN IRIDIUM WELD

The microbeam-Laue technique was applied to a complicated dislocation structure arising from plastic deformation in an Ir weld. Contraction of molten weld metal during solidification is resisted by colder surrounding metal, resulting in the appearance of stresses.[20] These stresses may partially relax by plastic deformation. As shown in the Laue patterns (Figs. 5–7), welding of polycrystalline Ir is accompanied by local plastic deformation as well as by residual stress. Microbeam-Laue diffraction reveals pronounced streaking of the Laue images from grains in the heat-affected zone. The plastic response of the material in the heat-affected zone can be described by the formation of geometrically necessary dislocations that appear in the material to relax the stress field induced during welding and subsequent cooling. In face-centered-cubic crystals, typical edge dislocation lines ''run'' parallel to the direction of ⟨112⟩ with Burgers vectors parallel to the direction ⟨110⟩ and with corresponding glide planes {111}.[16,17] There are 12 such systems for each crystal grain.

Laue images were made of different grains in the weld and in the heat affected zone and the orientation matrix for each grain was determined. In the center of the weld, Laue spots are sharp indicating that there is no residual plastic strain. In the heat-affected zone, large grains are observed

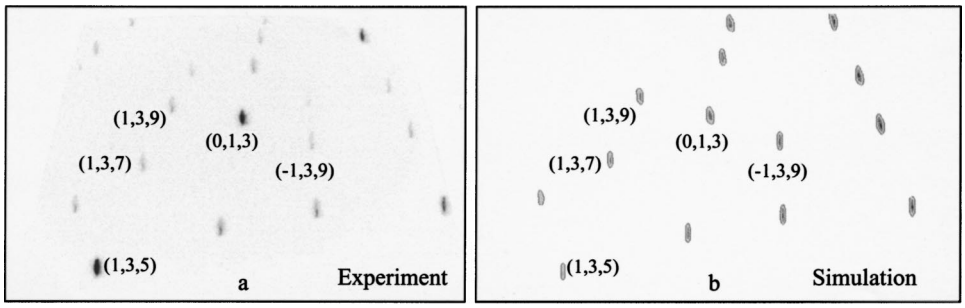

FIG. 5. Experimental (a) and simulated (b) Laue patterns from Ir weld in the heat-affected zone.

with significant deformation. Experimental and simulated Laue patterns are shown in Fig. 5. The orientation of the grain surface normal presented in Fig. 5(a) was almost parallel to [013]. In order to determine the orientation matrix of the grain more precisely, we chose three sets of three different reflections and determined the orientation matrix for each set. The final orientation matrix was obtained by averaging over those several sets. To understand the shape of the experimental Laue images and to check the sensitivity of the Laue image to different possible orientations of dislocations, we have chosen four reflections closest to the center of the Laue pattern (1,3,9), (1,3,7), (0,1,3), and $(-1,3,9)$ for this grain in the heat-affected zone [Fig. 5(a)]. We simulated their Laue images corresponding to 12 different slip systems of the primary GNDs (Fig. 6). The 12 most likely edge dislocation systems for this grain in the sample contribute distinct patterns to the beam spread. Analysis of those images indicates that only three of the slip systems give images that are close to the experimental one. Further analysis is performed by simulation of the whole Laue pattern and separate Laue spots for the above three possible slip systems. The qualitative and quantitative difference between the different dislocation systems allows identification of the active dislocation system [Fig. 5(b)]. It has Burgers vector $b=[011]$, dislocation line $\tau=[211]$, and slip plane $n=(111)$. We note that the intensity profiles of virtually all Laue spots are discontinuous, indicating the presence of GNBs. According to the Eq. (11), such a profile corresponds to the criterion $K\sim 1$. At least some of the GNDs are grouped into dislocation walls forming geometrically necessary boundaries. The presence of at least two pronounced GNBs separating three fragments in the irradiated volume is observed. Based on the analysis of experimental Laue spots we determined the misorientation angles between scattering fragments. These angles were then used as input parameters for the simulation. The best fit was obtained with simulations using three scattering fragments. The density of GNDs can be estimated by fitting the whole experimental Laue pattern as well as separate Laue spots by the simulated ones (Fig. 7). The contour map and intensity profiles along the ξ and ν directions of the streak are shown in Fig. 7(a) for reflection (135). Assuming same dislocation density and orientation of the activated slip system in each scattering fragment, we have simulated the whole 3D intensity portrait of several Laue spots and compared the simulated intensity profiles along and perpendicular to the streak with the experimental ones. After that, the best-fitting parameters for dislocation density, orientation of the slip system, exact positions, and misorientation angles through GNBs between scattering fragments were determined. Those misorientation angles between the central and neighboring fragments are equal to 0.25° and 0.35°, respectively. With the same set of parameters, we have recalculated both the whole Laue pattern [Fig. 5(b)], contour map for (135) reflection [Fig. 7(b)], and fitted the narrow and long slides along this Laue spot [Figs. 7(c) and 7(d)]. As a result, we have obtained a good fit to the experimental data. A transition from one

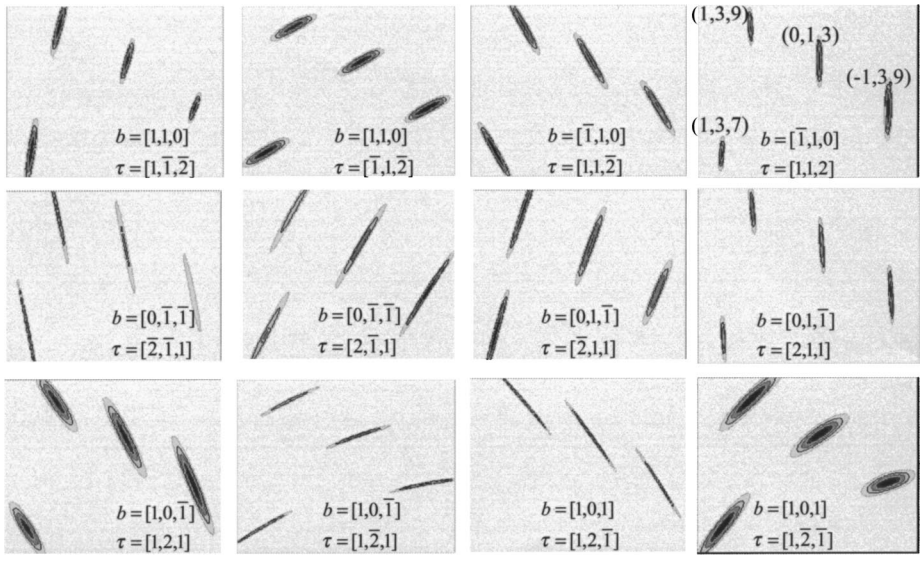

FIG. 6. Simulations of the (1,3,7), (1,3,9), (0,1,3), and $(-1,3,9)$ Laue spots near the central part of the Laue pattern for the 12 most likely slip systems defined by the Burgers vector **b** and dislocation line τ. One Laue image labeled with spot identification.

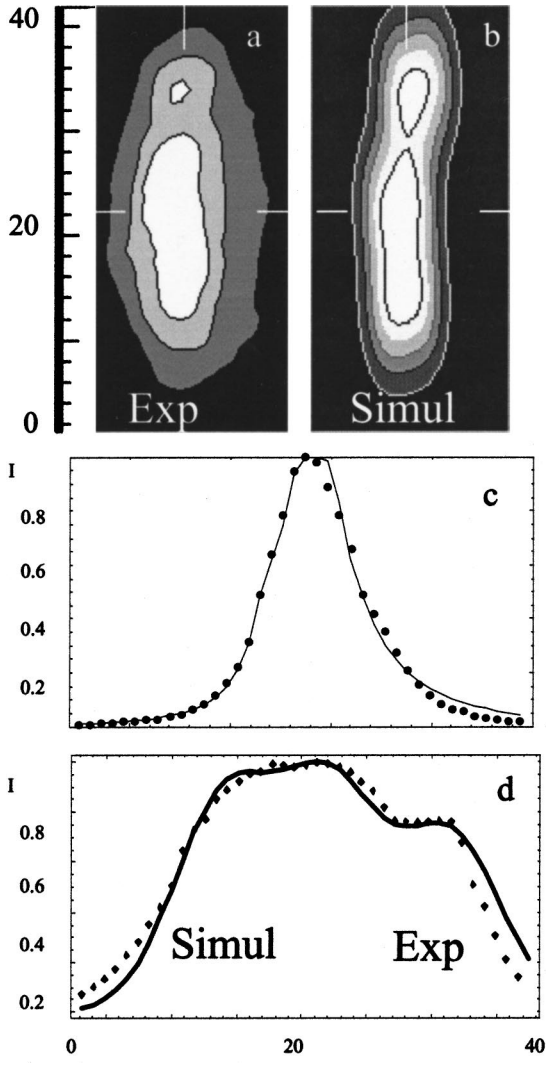

FIG. 7. Experimental (a) and simulated (b) contour maps of the (135) Laue spot and slices of intensity along ξ direction (c) and along ν direction (d). Several peaks are detected along ξ (dots, experimental data; solid lines, simulation).

dislocation network to another is observed at various positions in the weld. A detailed analysis of the hierarchical dislocation structure will be published after further investigation.

VI. SUMMARY

X-ray microdiffraction with broad-bandpass x-ray beams provides a powerful tool for the study of plastic deformation in materials. Plastic deformation, which results in a primary set of unpaired dislocations and dislocation walls produces elongated streaks in the Laue image that can be used to determine the dislocation density. The shapes of the intensity profiles along and perpendicular to the streak of the Laue spot allow for separation between unpaired random dislocations and unpaired dislocation boundaries. The predominant slip systems of the 12 most likely can be identified because of their distinctly different streaking of the Laue patterns. Misorientations of a heat-affected grain near a welded Ir joint were analyzed in terms of the dislocation and dislocation wall distribution and the operating slip systems.

ACKNOWLEDGMENT

This research was sponsored by the Division of Materials Sciences and Engineering, Office of Basic Energy Sciences, U.S. Department of Energy, under Contract No. DE-AC05-00OR22725 with UT-Battelle, LLC.

[1] G. E. Ice and B. C. Larson, Adv. Eng. Mater. **2**, 643 (2002).
[2] B. C. Larson, W. Yang, G. E. Ice, J. D. Budai, and J. Z. Tischler, Nature (London) **415**, 887 (2002).
[3] L. Margulies, G. Winther, and H. F. Poulsen, Science **291**, 2392 (2001).
[4] J. S. Chung and G. E. Ice, J. Appl. Phys. **86**, 5249 (1999).
[5] R. Barabash, G. E. Ice, B. C. Larson, G. M. Pharr, K.-S. Chung, and W. Yang, Appl. Phys. Lett. **79**, 749 (2001).
[6] D. P. Field and H. Weiland, *Electron Backscatter Diffraction in Materials Science* (Kluwer Academic, New York, 2002), pp. 199–212.
[7] G. K. Shenoy, P. J. Viccaro, and D. M. Mills, Report No. ANL-88-9, Argonne National Laboratory, IL (1988).
[8] N. Tamura, J. S. Chung, G. Ice, B. C. Larson, J. D. Budai, J. Z. Tischler, and M. Yoon, Mater. Res. Soc. Symp. Proc. **563**, 175 (1999).
[9] N. Tamura, R. S. Celestre, A. A. MacDowell, H. A. Padmpre, R. Spolenak, B. C. Valek, N. M. Chang, A. Manceau, and J. R. Patel, Rev. Sci. Instrum. **73**, 1369 (2002).
[10] E. M. Lauridsen, D. Juul Jensen, H. F. Poulsen, and U. Lienert, Scr. Mater. **43**, 561 (2000).
[11] M. Wilkens, T. Ungar, and H. Mughrabi, Phys. Status Solidi A **104**, 157 (1987).
[12] D. A. Hughes and N. Hansen, Acta Mater. **48**, 2985 (2000).
[13] F. R. N. Nabarro, *Theory of Crystal Dislocations* (New York, Dover Publications, 1987).
[14] M. A. Krivoglaz, *Theory of X-Ray and Thermal Neutron Scattering by Real Crystals* (Plenum, New York, 1996).
[15] R. Thomson and L. E. Levine, Acta Crystallogr., Sect. A: Found. Crystallogr. **53**, 590 (1997).
[16] D. A. Hughes, Q. Liu, D. C. Chrzan, and N. Hansen, Acta Mater. **45**, 105 (1997).
[17] F. J. Humphreys and M. Hatherly, *Recrystallization and Related Annealing Phenomena* (Pergamon, London, 1996).
[18] R. I. Barabash, Mater. Sci. Eng., A **309-310**, 49 (2001).
[19] J. Trenkler, R. Barabash, H. Dosch, and S. Moss, Phys. Rev. B **64**, 214101 (2001).
[20] I. C. Noyan and J. B. Cohen, *Residual Stress* (Springer, New York, 1987).